

Article

The Influence of Temperature on Degradation of Oil and Gas Tubing Made of L80-1 Steel

Dariusz Bęben 

Oil and Gas Institute—National Research Institute, 25A Lubicz Str., 31-503 Krakow, Poland; beben@inig.pl

Abstract: Corrosion in the oil and gas industry is very common due to the simultaneous action of a chemically active environment, temperature, and other non-chemical factors, for example, mechanical erosion by friction, and for these reasons corrosion is a very complex process. Corrosion at higher temperatures is an important aspect when extracting natural gas from a field with high temperatures (120 °C in the Lubiatow deposit and 180 °C in the gas well in Kutno). Water in the reservoir is often in the form of steam, with a pressure of about 25 MPa; as a result of its extraction, it cools down, which causes condensation. Condensed water in contact with the acid components of the gas causes corrosion, especially in the presence of aggressive gases, such as CO₂ and H₂S. Therefore, the aim of the work was to conduct research on the influence of water condensation, as a result of temperature changes in gasses containing CO₂ and H₂S on the corrosion of L80-1 steel at the junction of extraction pipes with casing pipes. The tests are carried out at temperatures of 65–95 °C, under a pressure of 7.5 MPa, so in quite aggressive conditions. The duration of the studies was 720 h (within a month). The results of the research allowed an answer to be provided for the question of what influence temperature, gas components, and pressure have on the corrosion of the well construction material. Moreover, the results clearly showed the selection of the material for the well, in order to prevent corrosion in aggressive environments.



Citation: Bęben, D. The Influence of Temperature on Degradation of Oil and Gas Tubing Made of L80-1 Steel. *Energies* **2021**, *14*, 6855. <https://doi.org/10.3390/en14206855>

Keywords: high temperature on corrosion of mining pipes; water; aggressive natural gas components; L80-1 steel

Academic Editor:
Marcin Kremieniewski

Received: 14 September 2021
Accepted: 14 October 2021
Published: 19 October 2021

Publisher's Note: MDPI stays neutral with regard to jurisdictional claims in published maps and institutional affiliations.



Copyright: © 2021 by the author. Licensee MDPI, Basel, Switzerland. This article is an open access article distributed under the terms and conditions of the Creative Commons Attribution (CC BY) license (<https://creativecommons.org/licenses/by/4.0/>).

1. Introduction

Water, in contact with the acid components of gas, causes corrosion in mining pipes. The pH of the reservoir water is affected by components of natural gas, such as CO₂ and H₂S [1–3]. The extension of the service life of pipelines requires engineering knowledge related to the degradation of the materials, the capability of the diagnostics of the corrosion (chemical) processes, and the analysis of numerical measurement data. The simultaneous presence of moisture (as an electrolyte) results in the accelerated corrosion of steel, more frequent pipeline failures, operational equipment damage, and environmental pollution [4–8]. The mechanism of the corrosion caused by the acid components of natural gas has been described and extensively studied. Steel, with the addition of chromium (Cr), is now the most frequently used metal, as it is resistant to the corrosion caused by the presence of CO₂ and H₂S. It was found that steel containing Cr (1 to 5%) increases the corrosion resistance almost ten-fold in comparison to that of carbon steels [3,9]. Therefore, steel with a low Cr content is used the most often. The research was aimed at studying the corrosion of chromium-containing (8%) steel at various temperatures. Despite numerous studies on the corrosion of steel with a low and high Cr content in the corrosive environment, there are no studies on the effect of temperature on the degradation process. The process of local electrochemical corrosion (pitting), which features a point mass loss, is related to the action of a local cell existing at the point of contact of the pipes [10]. The rate of metal dissolution at the point of contact of steels is very high, causing perforation of pipe walls in a very short time, without a bigger mass loss outside the attacked place. The pitting is intensified by

the aggressive chemical environment and the effect of high temperature. The presence of aggressive anions in the reservoir water, which feature high molar polarization, facilitates local damage to the passive layer [11]. In areas where the passive layer is the thinnest, a very large potential drop occurs, accelerating the permeation of ions, creating soluble chloride oxides through the oxide layer [12]. The pitting usually occurs on any internal inhomogeneities of the metal (non-metallic inclusions, precipitations, deformations), as well as on external inhomogeneities (edges, scratches, indentations, remnants of scale, deposits, etc.). The literature states that smooth and uniform surfaces are much more resistant to such corrosion [13]. The corrosion occurring in the environment of reservoir extraction is most frequently an example of chemical corrosion. The reaction of metal corrosion is a complex process and depends on the following factors:

1. Adsorption and chemisorption, that is, accumulation of substances originating from the gas on the metal surface, as a result of the formation of surface chemical connections with metal, creating a thin oxidation layer;
2. Origination of oxidation products on the absorption surface of the corrosion layer, and integrated into the crystalline lattice of the scale;
3. Diffusion/flow of metal ions to the formed scale.

The corrosion processes of oxidation depend on the pressure and temperature. Based on the literature, it is known that the corrosion rate of carbon steel under supercritical CO₂, without protective FeCO₃, is very high (≥ 20 mm/y) [14–18]. In certain conditions, the corrosion rate can decrease to low values (< 1 mm/y) during long-term exposure, due to the formation of a protective film of FeCO₃ [16–19]. A high pressure results in increased origination of pitting, and the corrosion rate may even be 20 times higher, due to a higher real pressure [20]. A layer of scale usually adheres to the metal, and cracks and microfissures exist close to the edge of the metal and scale. The formation of cracks and microfissures causes the start of a further pitting process. Increased pressure in the crack accelerates dissociation, forming a secondary phase of scale. The diffusion of oxidizer into the microfissures results in the formation of a second zone, and accelerates the internal corrosion. The rate of internal corrosion depends on the oxidising inclusions, metal composition, and cyclic temperature changes, and is the reason for the weakening of the mechanical properties, primarily metal plasticity and elasticity. One of the best corrosion protection solutions is now the application of an appropriate metal alloy and corrosion monitoring, and dosing inhibitors or cathodic protection.

To achieve corrosion protection, corrosion inhibitors are most frequently added to the reservoir water. They are already batched at the initial phase of production. During the extraction of natural gas with reservoir water, the investors seldom pay attention to the selection of an effective inhibitor to provide the best corrosion protection with varying pH of the fluid [21]. The temperature and pressure existing in the inter-tube space are also important parameters that affect the progression of the corrosion.

There are many methods of corrosion protection or the reduction in its effect, depending on the corrosion type and the chemical nature of the corrosive agents. The selection of an appropriate material for aggressive environment conditions, and the use of inhibitors to retard it, is the basic method of protection against chemical corrosion. The corrosive action of some agents may be substantially reduced by the use of corrosion inhibitors (retarders). On the metal surface, inhibitors usually form protective layers, which retard the corrosion rate. By definition, a corrosion inhibitor is a chemical agent, which, after application in small amounts, will effectively reduce corrosion. Laboratory tests should be carried out prior to the application of an inhibitor, whose action under conditions of high temperatures and pressures should then be checked. An inhibitor selected in such a way should effectively reduce the progression of the corrosion. A well-chosen inhibitor reduces the corrosion progression by approx. 95% with the use of 0.008% of the agent, and by 90% with the use of 0.004% of the agent [22]. The effectiveness of the agent usually depends on many factors, such as pressure, temperature, flow rate, and the composition, as well as on

the number of corrosive agents (water, CO₂, H₂S, NaCl, etc.) [23]. Inhibitors may conduct the following:

1. Creating a passivation layer on the surface via the growth of insoluble metal oxide on the surface. These bonds create a protective barrier coating, which becomes an impermeable layer, and, at the same time, it is very flexible and adheres well to the substrate [24]. Phosphates and chromates are typical examples of such an application;
2. Neutralising ions, which cause corrosion in the environment. Neutralising amines and ammonia are typical components of such an inhibitor. These are inhibitors that are effective in boiler waters and in slightly acid environments;
3. Removing caustic ions from the solution. In-hydrazine and sodium sulphate are typical components of the inhibitor. Such inhibitors remove oxygen dissolved in water.

2. Experimental Procedure

2.1. Methodology

The carried-out laboratory tests were aimed at determining the corrosion type occurring at the contact point of mining pipes and casing, proceeding as a result of temperature and reservoir water action. Laboratory tests on steel were carried out based on the schedule determined for specific solutions, determined temperatures and pressure. The samples of tested steel should be entirely immersed. The total test time was determined depending on the corrosion rate; for example, for samples whose corrosion rate, at an elevated temperature (calculated after 24 h), exceeds 0.3 mm/year, the test time should be at least 7 days, and at the rate below 0.3 mm/year—at least 30 days [25–29].

2.2. Materials

The tests were carried out using reservoir water containing CO₂ and H₂S, extracted from a well. Its composition is presented in Table 1 below.

Table 1. Composition of deposit water.

Variable	Value	Standard Deviation
Temperature [°C]	20.0	1.5
Density [g/cm ³]	1.182	0.001
pH	4.8	1.5
Eh [mV]	117.8	1.12
Carbonates [mg/dm ³]	n.s.	n.s.
Hydrogencarbonates [mg/dm ³]	152	15.6
Chlorides [mg/dm ³]	148.000	38.540
Calcium [mg/dm ³]	29.260	9.230
Magnesium [mg/dm ³]	5.350	1.320
Potassium [mg/dm ³]	590	62
CO ₂ [wt. %]	0.6	0.1
H ₂ S [wt. %]	0.15	0.01

The research was carried out using 16 different batches of water.

Plates of steel L80-1 were used for testing, with the composition as in Table 2, and with the dimensions 50 × 20 × 4 and 10 × 100 × 4 mm, cut out from a tube fragment (Figure 1).

Table 2. Chemical composition (wt. %) of L80-1 steel, norm ISO 11960 API 5CT.

C [%]	Mn [%]	Si [%]	P [%]	S [%]	Al [%]	Ni [%]	Mb [%]	Cr [%]	V [%]	Fe [%]
0.26	1.25	0.24	0.012	0.004	0.018	0.11	0.23	0.08	0.006	Bal.



Figure 1. Coupons used for testing.

The performed tests should determine the reason for pitting origination at various temperatures and in the reservoir water environment.

To study the corrosion of steel L80-1, depending on the temperature and corrosion time, visual inspection of the corroded samples surface was carried out as well as scanning microscopy and X-ray microanalysis of corrosion products. The view of geometrical structure of the corroded surface of samples was documented on a scanning microscope at diversified magnifications. X-ray microanalysis was carried out on the corroded surface in specific areas, marked with consecutive numbers. Metallographic microsections transverse to the corroded surface were made to determine the corrosion type and its progress depending on the adopted conditions. Upon that basis, the thickness of the layer of corrosion products on non-etched and etched microsections was evaluated, as was the shape of its external and internal boundary depending on the corrosion conditions. To evaluate the chemical composition, a linear qualitative analysis by means of X-ray microanalysis was carried out on the cross section of the corroded layer and steel substrate.

3. Results and Discussion

The research was carried out in a pressurized chamber (7.5 MPa) at 65, 80 and, finally, 95 °C for 720 h (30 days). The facility is shown in Figure 2. The tests were performed on steel L80-1. The tests were carried out in a level gauge type of chamber, which enabled observation of the samples during the test. The chamber was equipped with a manometer, in order to control the pressure during the tests, and a valve to maintain the pre-set pressure. Reservoir water was introduced into the chamber, as well as long samples, which were stacked up to observe the corrosion on the contact between the metals.



Figure 2. The chamber pressure tests.

As Figure 3 shows, all the samples taken out after the tests had a non-corroded top layer, which proves that a corrosion inhibitor was added to the reservoir water, preventing surface corrosion. At the metal/metal contact interface in Figure 3, a coat of dark brown–black bloom was observed, which proves that passivation occurs at the point of contact between metals. The observed passivation (surface corrosion) is a surface bloom; at a

temperature of 65 °C, it is difficult to remove, and at temperatures of 80 and 95 °C, it is poorly adhesive. No cases of pitting were observed upon visual inspection with the naked eye. The assessment of the steel surface was based on the microscopic examinations for the studied temperatures. The carried-out tests were aimed at determining the surface topography, microstructure, and the chemical composition of the top layer, as well as of the microstructure of the corroded samples. The chemical composition and surface topography were studied on an X-ray microanalyzer and a scanning microscope, at characteristic points of the corroded surface of the studied steel samples. The microstructure of the substrate material of long samples and the corrosion layer were studied on a Neophot 2 microscope [28]. Figure 4 shows, at the macro scale, the microstructures and chemical composition of the top layer, and the microstructures of the samples pressure-conditioned at 95 °C.

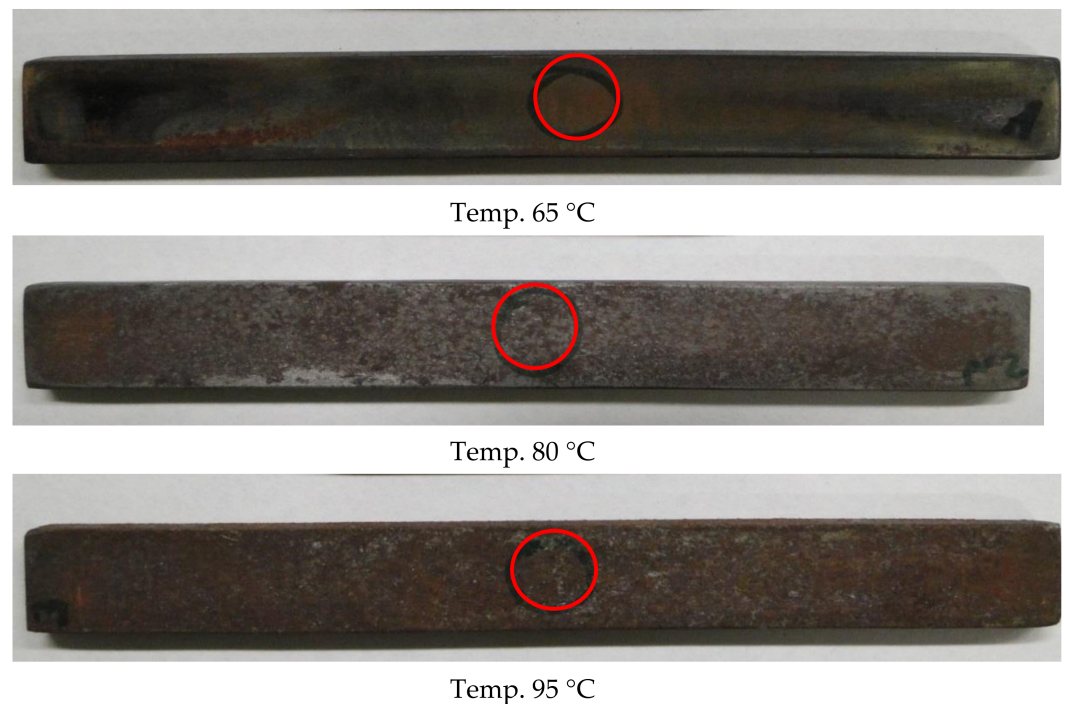


Figure 3. View of a coupon for research with selected places observed by SEM and EDS microanalysis.

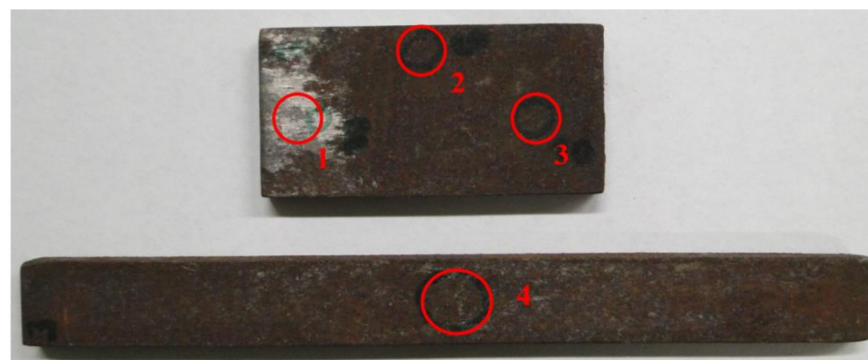


Figure 4. The samples prior to SEM/EDS analysis with indicated analysis points.

The topography of the sample surface (Figure 5) with visible craters is typical of pitting. The chemical composition determined on the surface of the studied sample showed a high oxygen and carbon content, which indicates the presence of iron oxides. As line 2 in Table 3 shows, the smallest steel loss was at this point; in the other points, 1 and 3, a high

amount of oxygen was observed, as well as a reduced amount of iron, which suggests the existence of iron oxides (corrosion products).

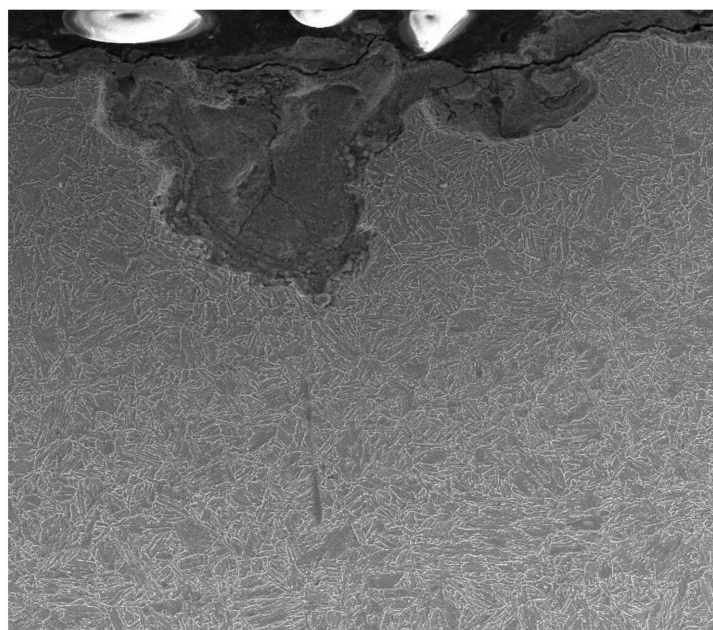


Figure 5. Cross section of L80-1 sample exposed to 95 °C (a long sample).

Table 3. EDS analyses for the sample indicated in Figure 6, the sample L80-1 exposed to 95 °C.

1.		Element	Wt. %	At. %
		O	9.88	27.57
		Cl	0.79	0.99
		Fe	89.33	71.44
		Total	100.00	100.00
2.		Element	Wt. %	At. %
		O	18.83	44.38
		Cl	0.72	0.96
		Fe	0.92	0.98
		Si	79.52	53.68
Total	100.00	100.00		
3.		Element	Wt. %	At. %
		O	16.17	40.00
		Cl	0.46	0.51
		Fe	82.59	58.52
		Si	0.57	0.81
		Cr	0.20	0.15
Total	100.00	100.00		
4.		Element	Wt. %	At. %
		O	17.60	41.31
		Cl	8.51	9.02
		Fe	73.89	49.68
		Total	100.00	100.00

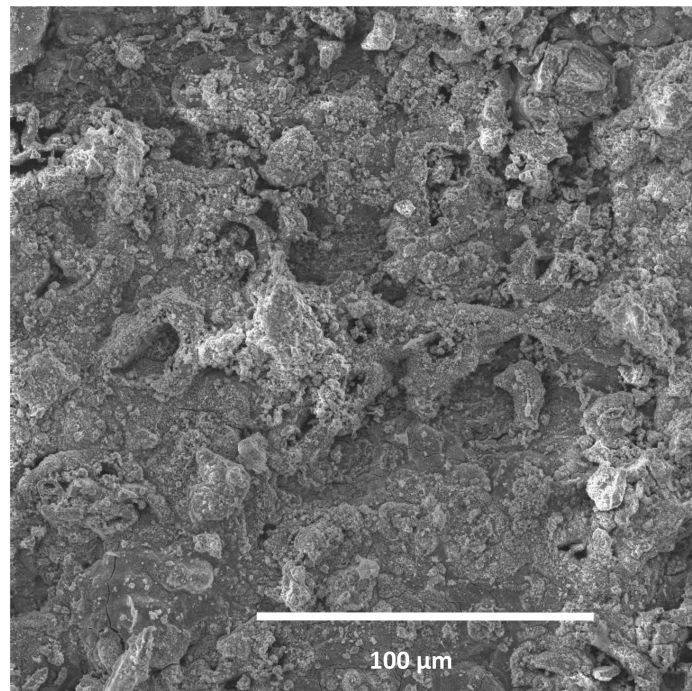


Figure 6. Cross section of L80-1 sample exposed to 95 °C corrosion scale (a long sample).

On metallographic microsections, transverse to the surface (Figure 6), the microstructure of the steel substrate of a sample fragment and a layer of corrosion products are visible. In the upper part, apart from visible pits, there is a black layer of corrosion products. The layer is porous, uneven, and cracked. The corrosive medium has access to the steel substrate via the unevenness, pores, and cracks. White inclusions are visible in certain places; this is a precipitated salt crystal, which integrated into the corrosion scale (Table 4). The majority of the studied sample is covered with scale, uniform corrosion, and single deep pits, 40 to 65 μm deep, visible under the microscope (Figure 7).

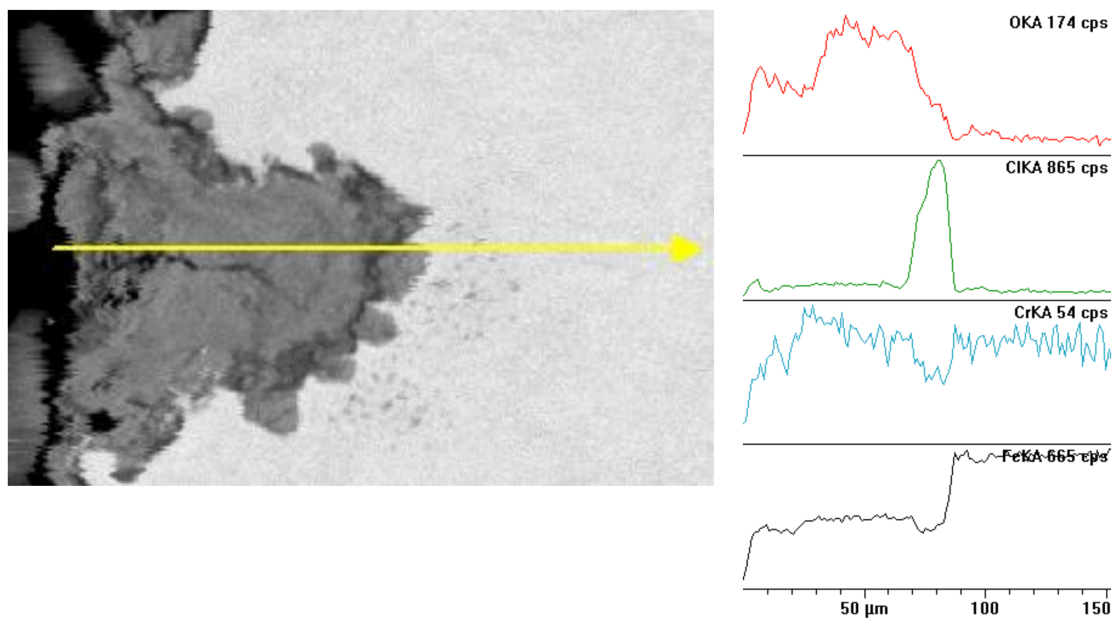


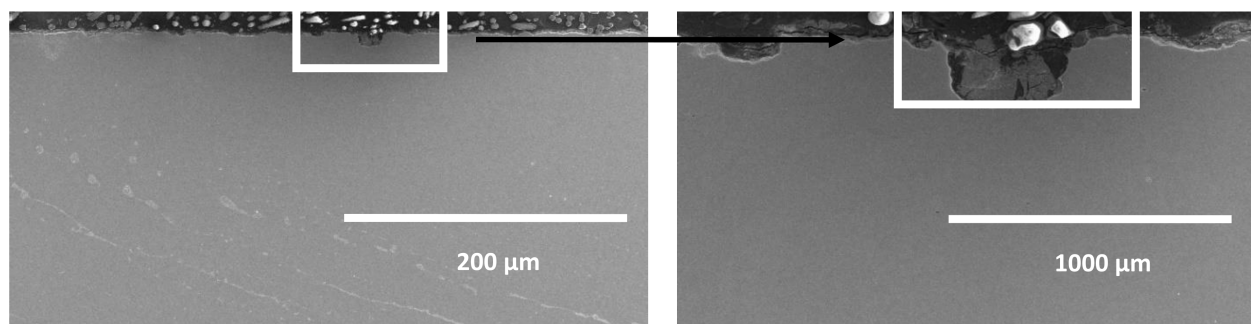
Figure 7. Cross section and linear cross scan of the elements in L80-1 steel at 95 °C.

Table 4. Results of chemical composition studies in the area from Figure 8.

Element	Wt. %	At. %
O	14.77	36.73
Cl	5.18	5.81
Fe	78.99	56.26
Si	0.60	0.85
Cr	0.46	0.35
Total	100.00	100.00

**Figure 8.** Topography studies of surface in Figure 7, microstructure and chemical composition of the top layer as well as the microstructure of the corroded sample, pressure-conditioned at 80 °C.

The metallographic micro-section, transverse to the surface, presented below (Figure 9), shows the microstructure of the steel substrate of a sample fragment and a layer of corrosion products. When comparing it with the samples conditioned at 80 °C, we can notice that the pits are larger and deeper. In the upper part, apart from visible small pits, as compared with 95 °C, there is a dark brown layer of corrosion products. This layer is porous and uneven. The corrosive medium has access to the steel substrate via the unevenness, pores, and cracks. White inclusions are visible in certain places; this is a precipitated salt crystal, which integrated into the corrosion scale. The majority of the studied sample is covered with scale and uniform corrosion, as well as cracks and single deep pits, approx. 25 to 30 µm deep, visible under the microscope; see Figure 10. At a temperature of 95 °C, the material was subjected to deeper destruction than at 80 °C.

**Figure 9.** Cross section of L80-1 sample exposed to 80 °C (a long sample).

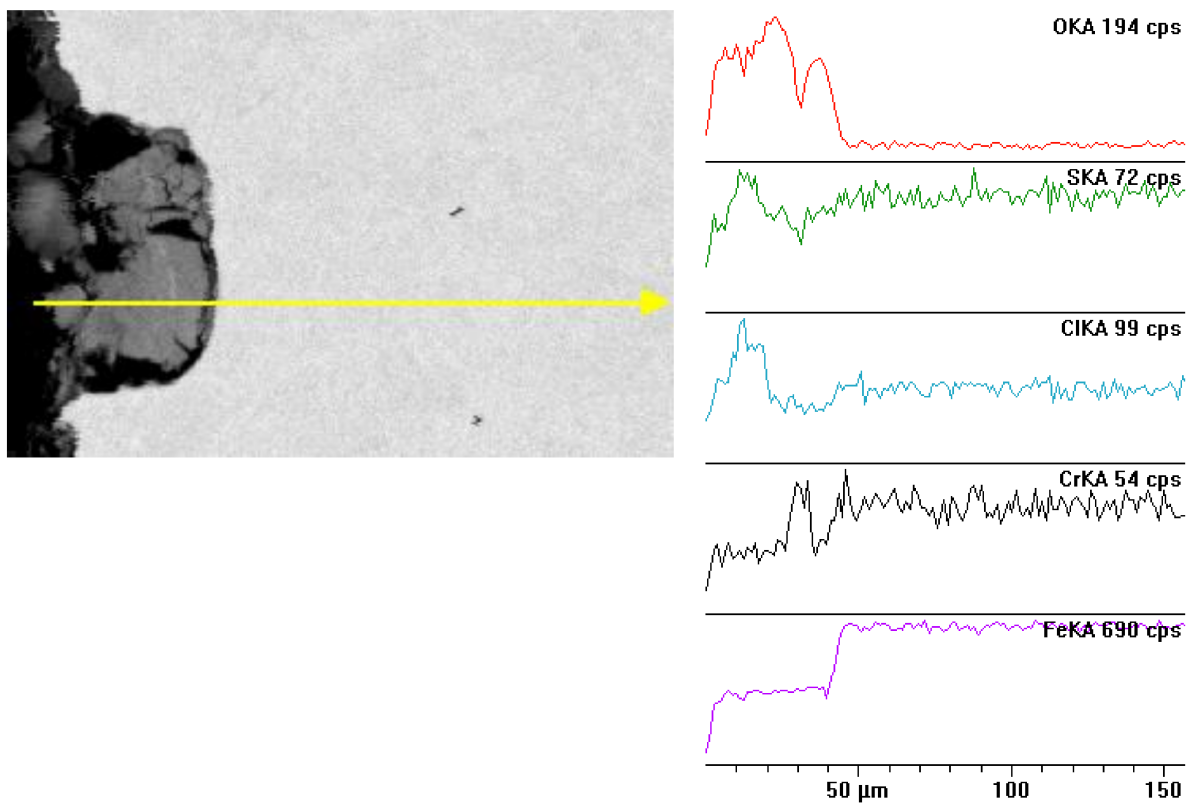


Figure 10. Cross section and linear cross scan of the elements in L80-1 steel at 80 °C.

White inclusions are visible in certain places; this is a precipitated salt crystal (see Figure 11), which integrated into the corrosion scale. The majority of the sample is covered with scale, uniform corrosion, and cracks that are visible under the microscope; there are no pits. Figure 12 shows the metallographic microsection transverse to the surface, with a visible microstructure of the steel substrate of a sample fragment and a layer of corrosion products. When comparing it with the samples studied at 95 and 80 °C, we can notice that there are no bigger pits. The surface is covered with a thin, relatively even black layer of corrosion products. The scale (the top layer of corrosion products) is approx. 10 to 12 μm thick. The surface was not subject to major destruction (see Figure 13), as compared with previously studied samples.

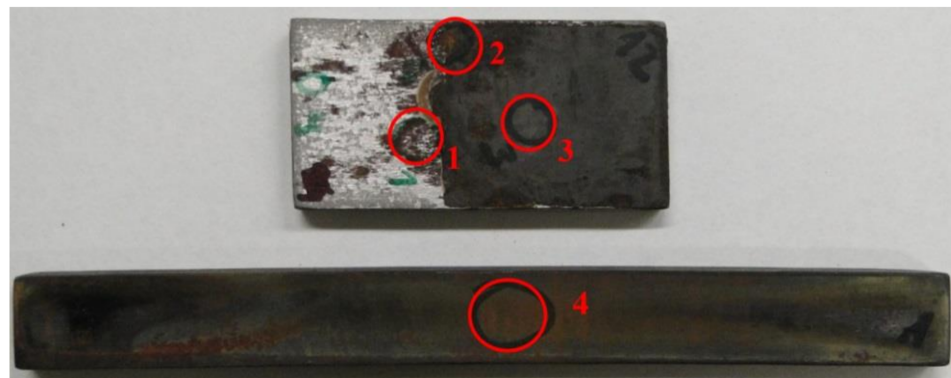


Figure 11. Macrostructure of the corroded sample at 65 °C.

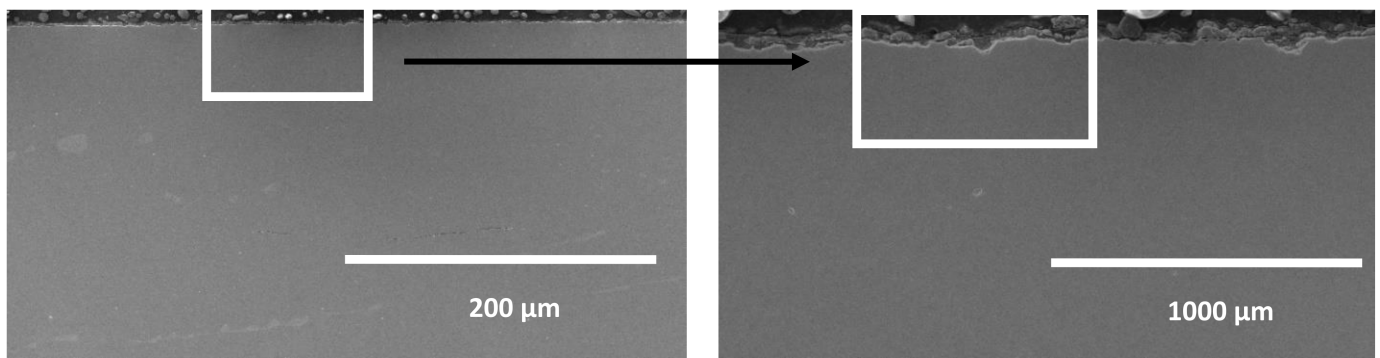


Figure 12. Cross section of L80-1 sample exposed to 65 °C (a long sample).

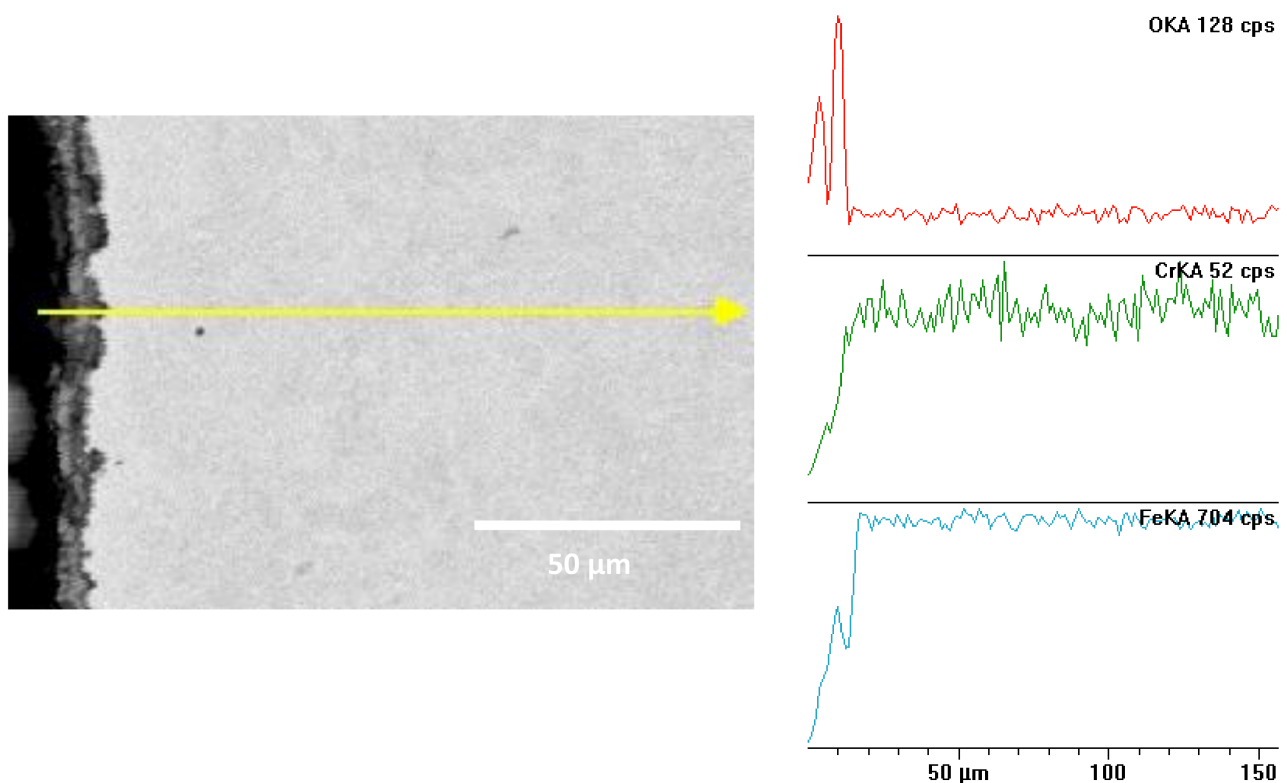


Figure 13. Cross section and linear cross scan of the elements in L80-1 steel at 65 °C.

Based on the obtained results, the occurrence of electrochemical corrosion was found in the tested samples, along with a propensity for pitting, resulting from the existence of chlorine ions from the reservoir water. The thickness of the layer of corrosion products, as well as the surface roughness and the pit depths, decrease with the reduction in temperature. At a temperature of 65 °C, a hard, rather thin adhesive layer of corrosion products forms. At the boundary with the steel substrate, practically no pits are observed. At 80 °C, and, in particular, at 95 °C, the corrosion layer is poorly adhesive, much thicker, and rough, with fractures and deep pits in the steel substrate. The existence of oxygen and chlorine was found in the corrosion layer. The chemical composition of the corroded layer, both on the surface and at the cross section, is uniform. The chlorine content is higher in the samples that corroded at a higher temperature. The tested steel L80-1 corrodes in the acid environment and at higher temperatures. The temperature plays a significant role in this case. The corrosion rate is affected by the type of product that forms under various temperature conditions. At low temperatures, iron and steel corrode, with the formation of a semi-protective layer of magnetite Fe_3O_4 on the surface, retarding the corrosion rate. The hitherto work shows that the corrosion rate of steel in CO_2 -saturated brine is initially

high, but it reduces over time, due to the formation of a siderite layer (iron II carbonate) of FeCO_3 on the surface (Zhang et al. 2013) [29,30]; studies were carried out that measured the loss of mass over time. In addition, H_2S has an adverse impact on the corrosion of steel, as was described by El Alami et al. (El Alami et al. 2011) [31]. At a temperature of $80\text{ }^\circ\text{C}$ on the surface of the steel, a microscopic, thin layer of oxides practically stops the process of iron release. Increasing the temperature to $95\text{ }^\circ\text{C}$ did not change the nature of the interactions and compounds, such as FeOH^+ , which are subject to adsorption to drive the dissolution at a rate that changes with time, and—as H_2CO_3 and H^+ are reduced—they proceed simultaneously at a slower rate, but extensive deep pits are observed; this is a particular type of corrosion, featuring a point loss of steel mass [32]. The course of pitting is related to the action of a local cell, which forms between a large, passivated surface of steel, being a cathode, and a local depassivated zone, being an anode. The rate of metal dissolution on the anode is very high, resulting in perforation in a very short amount of time, without a bigger mass loss outside the attacked place [33]. The pitting corrosion of steel occurs most frequently in water environments containing halide ions, i.e., chlorine, bromine, or iodine ions, where its intensity mainly depends on temperature and the concentration of ions [34]. It usually occurs on any internal inhomogeneities of the metal (non-metallic inclusions, precipitations, deformations), as well as on external inhomogeneities (edges, scratches, indentations, remnants of scale, deposits, etc.). Instead, smooth and uniform surfaces are much more resistant to such corrosion [4]. If iron is the damaged metal (the main component of steel), then the role of the corrosion-causing metal is fulfilled by carbon, contained in steel in the form of graphite grains, or iron carbide [35].

4. Conclusions

The studied steel L80-1 corrodes in an acid environment, and the corrosion is proportional to the increase in temperature, which plays a significant role. By monitoring the degradation processes of L80-1 steel, using modern tests, it is possible to detect the early stages of this degradation, such as the initiation and development of cracks near non-metallic inclusions, and the formation of CO_2 and H_2S -induced bubbles on the surface of the material. You will be able to observe the course of such processes in the future, and determine the period of safe operation of structures operating at different temperatures and in the environment. The corrosion rate is affected by the type of corrosion product, which forms at various temperatures. At lower temperatures, the tested steel corrodes, with the formation of a semi-protective layer of magnetite Fe_3O_4 and siderite FeCO_3 on the surface, retarding the corrosion rate. At a temperature of $80\text{ }^\circ\text{C}$, a microscopic, thin layer of oxides on the steel surface practically stops the process of iron release. When the temperature is $95\text{ }^\circ\text{C}$, the content of chlorides in the corrosive medium exceeds a critical value, the hitherto 'natural' anti-corrosion coat is damaged, and pitting corrosion occurs. Corrosion at lower temperatures is uniform (general) and consists of a uniform attack on the entire steel surface. As a result, the pipe thickness decreases uniformly, with a simultaneous reduction in general strength. The prevention of uniform corrosion effects (by reducing its rate) consists of exchanging the steel for a material with better corrosion resistance, periodical passivation of the steel surface, and the application of protection, e.g., cathodic, or appropriate protective coats and layers.

Funding: This research received no external funding.

Institutional Review Board Statement: Not applicable.

Informed Consent Statement: Not applicable.

Data Availability Statement: Data is contained within the article.

Conflicts of Interest: The author declare no conflict of interest.

References

1. Ribeiro, L.P.; Paulo, C.A.S.; Neto, E.A. Compos Basin-Subsea Equipment: Evolution and Next Steps. In Proceedings of the Offshore Technology Conference, Richardson, TX, USA, 5–8 May 2003; p. 15223.
2. Estrella, G. The Importance of Brazilian Deepwater Activities to the Oil Industry Technological Development. In Proceedings of the Offshore Technology Conference, Richardson, TX, USA, 5–8 May 2003; p. 15049.
3. Yougui, Z. Electrochemical Mechanism and Model of H₂S Corrosion of Carbon Steel. Ph.D. Thesis, Ohio University, Athens, GA, USA, 2015.
4. Mahmoodian, M.; Qingi, C. Failure assessment and safe life prediction of corroded oil and gas pipelines. *J. Pet. Sci. Eng.* **2017**, *151*, 434–438. [[CrossRef](#)]
5. Wang, W.; Natelson, R.; Stikeleather, L.; Roberts, W. CFD simulation of transient stage of continuous countercurrent hydrolysis of canola oil. *Comput. Chem. Eng.* **2012**, *43*, 108–119. [[CrossRef](#)]
6. Nestic, S. Key issues related to modelling of internal corrosion of oil and gas pipelines—A review. *Corros. Sci.* **2007**, *49*, 4308–4338. [[CrossRef](#)]
7. Revie, R. Oil, Gas Pipelines. In *Integrity and Safety Handbook*; John Wiley & Sons, Inc.: Hoboken, NJ, USA, 2015.
8. Papavinas, S. *Corrosion Control in the Oil and Gas Industry*; Elsevier: Houston, TX, USA, 2013.
9. Kermani, B.; Cochrane, R.; Dougan, M.; Linne, C.; Gonzalez, J. Development of low carbon Cr-Mo steels with exceptional corrosion resistance for oilfield applications. In Proceedings of the 56th NACE Annual Conference, Houston, TX, USA, 11–16 March 2001. Available online: <https://www.onepetro.org/conferencepaper/NACE-03117> (accessed on 13 October 2021).
10. Stachowicz, A. Korozja rur wydobywczyczych odwiertów gazowych zawierających CO₂. *Nafta-Gaz* **2011**, *11*, 395–400. (In Polish)
11. Zhang, G.A.; Liu, D.; Li, Y.Z.; Guo, X.P. Corrosion behavior of N80 carbon steel in formation water under dynamic supercritical CO₂ condition. *Corros. Sci.* **2017**, *120*, 107–120. [[CrossRef](#)]
12. Stachowicz, A. Korozja rur w odwiertach oraz dobór ochrony inhibitowanej w płynach nadpakerowych. *Nafta-Gaz* **2013**, *7*, 525–531. (In Polish)
13. Atiwat, K. Lifetime Estimation of Steel Tubing by Corrosion Analysis for Petroleum. Master's Thesis, Geotechnology Suranaree University of Technology, Nakhon Ratchasima, Thailand, 2016.
14. Choi, Y.S.; Young, D.; Nestic, S. Effect of Impurities on the Corrosion Behavior of CO₂ Transmission Pipeline Steel in Supercritical CO₂-Water Environment. *Environ. Sci. Technol.* **2010**, *44*, 9233–9238. [[CrossRef](#)] [[PubMed](#)]
15. Choi, Y.S.; Nestic, S. Determining the Corrosive Potential of CO₂ Transport Pipeline in High pCO₂-Water Environments. *Int. J. Greenh. Gas Control* **2011**, *5*, 788. [[CrossRef](#)]
16. Zhang, Y.; Pang, X.; Qu, S.; Gao, X.; Li, K. The relationship between fracture toughness of CO₂ corrosion scale and corrosion rate of X65 pipeline steel under supercritical CO₂ condition. *Int. J. Greenh. Gas Control* **2011**, *5*, 1643–1650. [[CrossRef](#)]
17. Zhang, Y.; Pang, X.; Qu, S.; Gao, X.; Li, K. Discussion of the CO₂ corrosion mechanism between low partial pressure and supercritical condition. *Corros. Sci.* **2012**, *59*, 186–197. [[CrossRef](#)]
18. Suhor, M.F.; Mohamed, M.F.; Nor, A.M.; Singer, M.; Nestic, S. Corrosion of mild steel in high CO₂ environment: Effect of the FeCO₃ layer. In Proceedings of the Corrosion 2012, Salt Lake City, UT, USA, 11–15 March 2012; p. 0001434.
19. Cui, Z.D.; Wu, S.L.; Zhu, S.L.; Yang, X.J. Study on Corrosion Properties of Pipelines in Simulated Produced Water Saturated with Supercritical CO₂. *Appl. Surf. Sci.* **2006**, *252*, 2368. [[CrossRef](#)]
20. Osokogwu, U.; Oghenekaro, E. Evaluation of corrosion inhibitors effectiveness in oilfield production operations. *Int. J. Sci. Technol. Res.* **2012**, *1*, 19–23.
21. Banaś, J.; Mazurkiewicz, B.; Solarski, W. Problem korozji mikrobiologicznej w instalacjach geotermalnych. *Ochr. Przed Korozją* **2011**, *3*, 76–81. (In Polish)
22. Bęben, D. Ochrona chemiczna metali przed korozją na przykładzie wybranych kopalń gazu ziemnego. *Ochr. Przed Korozją* **2014**, *12*, 478–481. (In Polish)
23. Bęben, D. Badania skuteczności działania wybranych inhibitorów korozji stosowanych okresowo w przemyśle wydobywczym. *Ochr. Przed Korozją* **2019**, *62*, 376–381. (In Polish)
24. PN-70/H-04600 Korozja metali. Badanie odporności korozyjnej metali i stopów. Ogólne wytyczne. (In Polish)
25. PN-76/H-04601 Korozja metali. Badania laboratoryjne w cieczach i roztworach w temperaturze otoczenia. (In Polish)
26. PN-78/H-04608 Korozja metali. Skala odporności metali na korozji. (In Polish)
27. PN-78/H-04610 Korozja metali. Metody oceny badań korozyjnych. (In Polish)
28. Młynarski, A.; Piasecki, A.; Jakubowski, J. Badania mikroskopowe i strukturalne skorodowanych próbek stali L80-1. *Politech. Poznańska. Poznań* **2012**, 699–702. (In Polish)
29. Zhang, X.; Zevenbergen, J.; Benedictus, T. Corrosion Studies on Casing Steel in CO₂ Storage Environments. *Energy Procedia* **2013**, *37*, 5816–5822. [[CrossRef](#)]
30. Eliyan, F.F.; Alfantazi, A. Influence of temperature on the corrosion behavior of API-X100 pipeline steel in 1-bar CO₂-HCO₃⁻ solutions: An electrochemical study. *Mater. Chem. Phys.* **2013**, *140*, 508–515. [[CrossRef](#)]
31. El Alami, H.; Augustin, C.; Orleans, B.; Servier, J.J. Carbon Capture and Storage projects: Material integrity for CO₂ injection and storage. *Eurocorr* **2011**, *2011*, 4741.
32. Choi, Y.S.; Farel, F.; Nešić, S.; Magalhães, A.A.O.; Andrade, C.D.A. Corrosion behavior of deep water oil production tubing material under supercritical CO₂ environment: Part 1-effect of pressure and temperature. *Corrosion* **2014**, *70*, 38–47. [[CrossRef](#)]

33. Jakubowski, M. Influence of pitting corrosion on fatigue and corrosion fatigue of ship structures Part I Pitting corrosion of ship structures. *Pol. Marit. Res.* **2014**, *81*, 62–69. (In Polish) [[CrossRef](#)]
34. Li, D.; Liu, Q.; Wang, W.; Jin, L.; Xiao, H. Corrosion Behavior of AISI 316L Stainless Steel Used as Inner Lining of Bimetallic Pipe in a Seawater Environment. *Materials* **2021**, *14*, 1539. [[CrossRef](#)] [[PubMed](#)]
35. Zhang, D.; Gao, X.; Li, W.; Li, B.; Guo, J.; Zhang, J.; Pang, Q.; Xu, Z. CO₂ corrosion behavior of high-strength martensitic steel for marine riser exposed to CO₂-saturated salt solution. *Mater. Res. Express* **2021**, *8*, 076517. [[CrossRef](#)]